Robust Fringe Pattern Analysis Method for Transient Phenomena

Mariano Rivera[a,b*]

[a]*Centro Nacional de Supercomputo, IPICYT, San Luis Potosi, SLP. 78216, Mexico*
[b]*Centro de Investigacion en Matematicas AC, Guanajuato, Gto. 36000, Mexico*

Abstract

We propose a method for analysing a sequence of noisy interferograms with closed fringes acquired at a high–speed frame rate. Our method is appropriate for analysing ESPI sequences of transient phenomena such as deformations caused by vibrations. Firstly, we compute a differential phase between frames using a procedure based on a Gabor filter bank. We then refine this initial phase with a regularised quadratic cost function that keeps the consistency of the restored phase with the fringe patterns. In addition, we also present the robust version of our phase refining method. This prevents the introduction of phase deformations by the smoothing process. We demonstrate by means of numerical and real–data experiments that our method is appropriate for analysing ESPI sequences of transient phenomena.

Keywords: Imaging ultrafast phenomena, Fringe analysis, Speckle interferometry, Optical metrology, Vibration analysis, Two phase step methods, Gabor filter bank, Robust image processing.

1. Introduction

We present a method for analysing transient, or dynamic, phenomena with interferometric techniques; examples of such deformations are given by vibrations [1, 2]. In particular, we are interested in the case in which the studied object is under dynamic deformation and yields a spatial–variable phase shift in the Fringe Pattern (FP). A popular method for generating FPs in the study of transient phenomena for industrial applications is the so-called Electronic Speckle Pattern Interferometry (ESPI) technique [1, 2, 3]. Advances in video cameras have allowed the implementation of high–speed ESPI systems for acquiring FP sequences of transient phenomena at frame rates of 1 kHz [4, 5, 6], or superior [8].

In this work, we assume adverse experimental conditions that produce time and spatial variations in the unknown background illumination and local fringes' contrast; for example, those characteristics are present in the simple synthetic interferograms shown in Panels (a) and (b) in Figure 1 (the remaining panels will be described latter). The mathematical model of the FP sequences we analyse is given by

$$I_k(x) = a_k(x) + b_k(x)\cos(\phi_k(x) + k\delta) + \eta_k(x), \qquad (1)$$

where the vector $x \in \mathbb{Z}^2$ denotes the pixel position in a regular lattice $\mathcal{L}$ and we assume a constant phase shift, δ, between consecutive FPs indexed by k (time). The background illumination and the local fringe contrast are denoted by a and b, respectively. Finally, η is the residual.

---

*Corresponding author

Email address: (`mariano.rivera@ipicyt.edu.mx`, `mrivera@cimat.mx`) (Mariano Rivera[a,b])

We use the general definition of residuals: the differences between the truth data (observed or ideal) and the best prediction with the fitted model. Such a residual is product of noise in the data (observation residual), model bias (the model limitations) and estimation residual, (associated with the numerical method solver) [7]. In the case of ESPI, the noise is correlated with the FP's intensity [2, 9].

In our model (1), we have a phase, ϕ, that depends on time k, as opposed to classical phase stepping algorithms where the phase ϕ is kept constant [10]. An algorithm that analyses the simpler case of a temporal constant phase and unknowns phase steps is reported in [11]. In order to analyse sequences of FP with temporal variable phase, there are techniques based on special experimental setups that simultaneously acquire a set of phase shifted FPs [12, 8]. Thus, a transient phenomenon can be analysed by acquiring an evolution sequence of a set of phase shifted FPs. The drawbacks of such a technique are the complexity of the experimental setup and the resulting reduction in the FP's spatial resolution [8]. Other configurations use RGB colour codification for generating three simultaneously phase shifted FPs [3].

We simplify the experimental setup by acquiring a sequence of single FPs (with temporally variable phase) with known phase shifts, $k\delta$. Herein we present a method for computing the differential phase between contiguous FP in the sequence. Our method assumes that the FP sequence is acquired at a high–speed rate such that the local fringes' shift is in the interval $[0, \pi)$. This experimental condition allows us to compute an initial solution for the differential phase that we refine afterwards.

We organise this paper as follows. We present our two–stages method in section 2. In subsection 2.1 we present

the stage for computing the initial solution for the phase variation with respect to time. Afterwards, in subsection 2.2, we present the stage in which we refine such an initial solution. In subsection 2.3, we propose a robust variant of our refinement process that fits for cases where the initial differential phase estimate is corrupted with outliers. In section 3, we present a discussion on related work and techniques. More specifically, subsection 3.1 shows the relationship between our approach based on a Gabor filter bank [13] and the Short-Term Fourier Transform [14]; and subsection 3.2 contrasts our refining solution versus simple phase filtering approaches. In section 4, we present numerical and real experiments that demonstrate the suitability of our method for analysing ESPI sequence of transient phenomena. Finally, our conclusions are given in section 5.

2. Method

2.1. Computing the initial time–differential phase

Let $\{I_k\}_{k=1,2,\ldots,K}$ be a sequence of FPs. We define the differential phase sequence $\{\mathbf{f}_k\}_{k=2,\ldots,K}$ as follows:

$$\mathbf{f}_k(x) \stackrel{def}{=} \phi_k(x) - \phi_{k-1}(x) \qquad (2)$$

where $[\phi_k, \phi_{k-1}]$ are the phases of $[I_k, I_{k-1}]$, respectively. In this context, $\mathbf{f}_k$ is a spatial–variant phase that codifies the information of the transient phenomena of interest.

When analysing transient phenomena, one is interested in computing the variation of the phase with respect to time. In the framework of inverse problem solutions, one needs to define the relationship between the observed data and the unknown variables by means of an observation model. For example, the model (1) establishes the relationship between the observed FP I_k and the unknown phase ϕ_k. A possible way to compute the phase differences (2) is to estimate a solution to the inverse problem stated by the model (1). That is, to estimate the phase ϕ_k for each FP using a general single closed FP algorithm [15, 16, 17, 18, 19, 20, 21]. The inconvenience of such a strategy is that closed FP analysis procedures are of propagating type are prone to fail with either noisy FP, or relatively large constant regions, or variations in the illumination conditions. Therefore, before using a closed FP analysis method, the FPs are frequently preprocessed in order to filter out noise and normalise their illumination components. Since methods build upon the propagation of a seed solution with a flood-fill strategy, their computational efficiency depends on the image dimension; i.e., the pixels should sequentially be updated.

Our approach can be related to methods that compute the global phase step between two interferograms when the phase shift is unknown [13, 22, 23]. However, we compute a spatially variable phase shift.

First, we compute the magnitude, $\mu_k(x)$, and phase, $\psi_k(x) \in [-\pi, \pi)$, of each FPs (for $k = 1, 2, \ldots, K$) at each
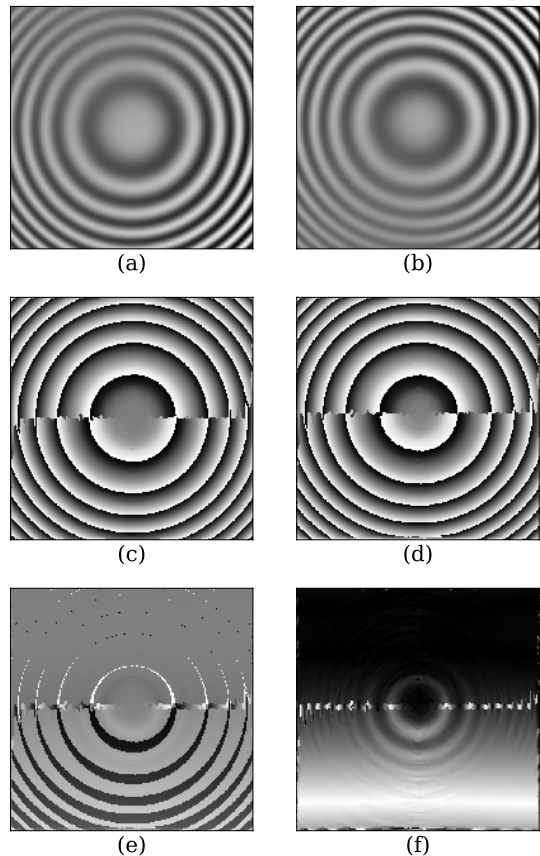
Figure 1: Summary of the procedure to estimate the initial differential phase. Fringe patterns: a) I_k and b) I_{k-1}. Local phases computed with the GFB: c) ψ_k and d) ψ_{k+1}. e) Phase differences map: $g_k = \psi_k - \psi_{k-1}$. f) Initial differential phase $\tilde{f}_k = |\mathcal{W}\{g_k\}|$.

pixel ($\forall x \in \mathcal{L}$) using the operator $\mathcal{H}$:

$$\{\mu_k, \psi_k\}(x) = \mathcal{H}\{I_k\}(x). \qquad (3)$$

According to [13] and using our model (1), the computed local phase, ψ, follows the model

$$\psi_k(x) = \mathcal{W}\{s_k(x)[\phi_k(x) + k\delta] + \tilde{\eta}_k(x)\}; \qquad (4)$$

where $\mathcal{W}$ is the wrapping operator, $\tilde{\eta}_k$ is a residual with zero mean and $s_k \in \{-1, 1\}^{\sharp \mathcal{L}}$ is a random sign map. Since η in (1) is assumed white noise(i.e., it has all the frequency components), then $\tilde{\eta}$ are the noise components that pass through the Gabor Filter.

In this work we implemented $\mathcal{H}$ using a Gabor Filter Bank (GFB) as is reported in [13], see section 3.1. The noise reduction and illumination components' normalisation are implicit in the GFB.

The next proposition introduces a subrogate model that relates the computed phases ψ_k and ψ_{k-1} with the unknown differential phase $\mathbf{f}_k$.

Proposition 1. Let g_k be the simple differences map computed as

$$g_k(x) \stackrel{def}{=} \psi_k(x) - \psi_{k-1}(x). \qquad (5)$$

The relationship of g_k with the unknown differential phase $\mathbf{f}_k$ is given by

$$\mathcal{W}\{g_k(x)\} = s_k(x)[\mathbf{f}_k(x) + \delta] + \hat{\eta}_k(x) + 2\pi\, n_k(x); \quad (6)$$

where $2\pi n_k$ factor is by the wrapping operator and

$$\hat{\eta}_k(x) \overset{def}{=} [s_k(x) - s_{k-1}(x)][\phi_{k-1}(x) + (k-1)\delta] + \tilde{\eta}_k(x) - \tilde{\eta}_{k-1}(x) \quad (7)$$

can be understood as a new residual that absorbs the remainders that results of the phase estimations by the GBF (4) and introduced by the change in the sign map $(s_k - s_{k-1})$.

Details of the proof of Proposition 1 are presented in Appendix A.

Formula (6) can be understood as a surrogated model that explains the indirect observations, g_k, from the unknowns, $\mathbf{f}_k$ and s_k. Unfortunately, such a problem is still difficult to solve because it is nonlinear (product of the unknowns fields, the effect of the wrapping and absolute-value operators) and has correlated residual. In order to simplify model (6), we impose some conditions on the experimental setup; *i.e.*, in the acquisition protocol.

Proposition 2. *Assume that known constant phase shift, δ, and the high–speed acquisition rate are such that*

$$\mathbf{f}_k(x) + \delta \in [0, \pi). \quad (8)$$

Thus, the absolute value of (5),

$$f_k(x) \overset{def}{=} |\mathcal{W}\{g_k(x)\}|,$$

results in the simplified model:

$$f_k(x) = \mathbf{f}_k(x) + \delta + r_k(x); \quad (9)$$

where the new residual r_k satisfies $0 \le \mathbf{f}_k + \delta + r_k \le \min\{\pi, \mathbf{f}_k + \delta + |\hat{\eta}_k + 2\pi\, n_k|\}$ and has an important contribution of the correlated residual $(s_k - s_{k-1})$.

Details of the proof of Proposition 2 are presented in Appendix A.

We note that the sign map s_k is related to the local orientations of the fringes and the GFB design. The constant fringe shift δ between FPs keeps the local frequency constant and, consequently, does not affect the sign map. At high acquisition rate of the FP sequence, the transient phenomenon will introduce small changes in the fringe's orientation that could produce slight changes in the sign map (*i.e.*, $s_k \approx s_{k-1}$):

$$|\hat{\phi}'_k(x) - \hat{\phi}'_{k-1}(x)| \approx 0, \forall x \rightarrow s_k \approx s_{k-1} \quad (10)$$

where $\hat{\phi}'_k = \nabla\phi_k / \|\nabla\phi_k\|$ is the normalised spatial gradient of the kth FP.

Thus, from Propositions 1 and 2, our problem is cast by our simplified model (9) as: the estimation of the shifted–differential phase $\mathbf{f}_k + \delta$, with $\delta \in [0, \pi/2)$ known, given the observed (computed) differential phase

$$f_k = |\mathcal{W}\{\psi_k(x) - \psi_{k-1}(x)\}|. \quad (11)$$

Figure 1 shows two FPs (I_k and I_{k-1}); the computed local phase maps (ϕ_k and ϕ_{k-1}); the phase difference $\phi_k - \phi_{k-1}$ and the estimated initial differential map, f_k. Observe that large residuals appear in regions close to the places where the sign changes occur.

2.2. Refining the time–differential phase

Now, we compute an additive correction map p_k, to the initial differential phase f_k, to obtain a refined differential phase $\hat{f}_k$:

$$\hat{f}_k(x) = f_k(x) + p_k(x). \quad (12)$$

We compute the correction map p_k as the minimiser of a regularised cost function of the general form

$$p_k = \underset{p}{\arg\min}\, D(p; \psi_k, \psi_{k-1}, f_k) + \lambda R(p; f_k), \quad (13)$$

where the data attachment term D promotes consistency of the refined differential phase $\hat{f}_k$ and the computed local phases ψ_k and ψ_{k-1}. The regularisation term R induces the refined differential phase to be smooth. The positive parameter λ controls the relative weight of both terms.

Since the local phases (ψ_k and ψ_{k-1}) are wrapped and are multiplied by their respective random–signs maps (s_k and s_{k-1}), we need an agnostic function to such drawbacks. That in order to build the data term that reflects the desired consistency among (ψ_k, ψ_{k-1}) and $f_k(x) + p_k(x)$. Then, the initial version of our data term is:

$$\sum_{x \in \mathcal{L}} [\cos(f_k(x) + p_k(x)) - \cos(\psi_k(x) - \psi_{k-1}(x))]^2. \quad (14)$$

Moreover, we assume that the correction to the initial estimate phase is small enough ($|p_k(x)| < 1$) such that we can use an expansion based on the Taylor series of the first order for the second term in (14):

$$\cos(f_k(x) + p_k(x)) \approx \cos(f_k(x)) - p_k(x)\sin(f_k(x)). \quad (15)$$

Now, we define

$$C_k(x) \overset{def}{=} \cos(f_k(x)) - \cos(\psi_k(x) - \psi_{k-1}(x)) \quad (16)$$

$$S_k(x) \overset{def}{=} \sin(f_k(x)). \quad (17)$$

It is important to note that if f_k corresponds to 11, one can cancel the term C_k. However, this is not the case if one uses a filtered version of f_k, as we will see afterwards; for the moment, we will keep it in our formulation. Hence, using these definitions, we substitute (15) into (14) and

3

rewrite the data term (14). Hence, our final version in order to compute p_k is a regularised quadratic cost function:

$$p_k = \underset{p}{\arg\min} \sum_{x \in \mathcal{L}} \left\{ \left[C_k(x) - S_k(x)p(x) \right]^2 + \gamma\, p(x)^2 \right.$$
$$\left. + \lambda \sum_{x' \in \mathcal{N}_x} \left[f_k(x) + p(x) - f_k(x') - p(x') \right]^2 \right\};$$
$$(18)$$

where

$$\mathcal{N}_x = \{ x' \in \mathcal{L} : \| x - x' \| = 1 \}$$

is the set of first neighbour pixels of the pixel x. The first term in (18) enforces the correction map to be consistent with a phase difference model. The second term, weighted by the positive parameter γ, enforces the reduction of the magnitude of $p(x)$. The third term in (18) induces smoothness in the differential phase map.

Since our cost function (18) is quadratic and convex, one has several methods to chose from to solve the optimisation problem. A simple and memory efficient procedure is the iterative Gauss-Seidel scheme with the updating formula:

$$p(x) = \frac{S_k(x)C_k(x) + \lambda \sum\limits_{x' \in \mathcal{N}_x} \left[f_k(x') + p(x') - f_k(x) \right]}{S_k(x)^2 + \lambda\,\sharp\mathcal{N}_x + \gamma},$$
$$(19)$$

where we use the symbol $\sharp$ for cardinality. Note that, given that the correction terms p_k's are mutually independent, then they can be updated in any order. Moreover, we choose to update the pixels with formula (19) from left to right and top to down order; however, it is well-known that Gauss-Seidel does not imposes a particular updating order for updating.

Since we penalised the magnitude of p in order to keep valid the first Taylor series approximation (15), then we may require of the accumulation of several small refinement to achieve large phase corrections. Let $\hat{f}_k \leftarrow \text{Refine}(\psi_k, \psi_{k-1}, f_k)$ be our phase refining process, then we can iterate the refinement to improve the updated phase using

$$\hat{f}_k \leftarrow \text{Refine}(\psi_k, \psi_{k-1}, \hat{f}_k). \qquad (20)$$

Note that we are using a previously refined phase as parameter to our Refine($\cdot$) process, then the term C_k (16) is not zero. This iterative refinement converges rapidly and therefore we use only six iterations in our experiments. This iterative procedure is presented in Algorithm 1.

2.3. Robust refining the time–differential phase

In the analysis of transient phenomena for industrial applications by ESPI techniques, it is common to have experimental setups that produces low quality FP sequences: low contrast, inhomogeneous background illuminations, low frequency regions and high levels of noise. This characteristics produces that the computed phase with the GFB

Algorithm 1 Refine the differential phase between two consecutive frames

Require: The local phase of the consecutive frames (ψ_k, ψ_{k-1}), the estimate of the differential phase f and parameters of the refinement (λ, γ), the number of iterative refinements N.
1: **function** REFINE($\psi_k, \psi_{k-1}, f, \lambda, \gamma, N$)
2:     Let $\mathcal{L}$ be the set of pixels positions in the kth frame
3:     **for** $t = 1 : N$ **do**
4:         Compute C_k with (16)
5:         Compute S_k with (17)
6:         **repeat**
7:             Update $p_k(x)$ for $x \in \mathcal{L}$ with (19)
8:         **until** convergence
9:         Update the differential phase $f_k = f_k + p_k$
10:     **end for**
11:     **return** the refined phase f_k
12: **end function**

---

would be incorrect at some pixels; *i.e.*, the filter with maximum response is detuned with the FP's local-frequency. In order to eliminate the contribution of initial differential phases that uses detuned estimations of local phases, we become robust our refinement energy. In particular, we transform our refinement to the half-quadratic regularisation variant [24, 25]:

$$p_k, w_k = \underset{p,w}{\arg\min} \sum_{x \in \mathcal{L}} \left\{ V\big(C_k(x) - S_k(x)p(x) \big) + \gamma\, p(x)^2 \right.$$
$$\left. + \lambda \sum_{x' \in \mathcal{N}_x} \left[f_k(x) + p(x) - f_k(x') - p(x') \right]^2 \right\};$$
$$(21)$$

where V is a robust and convex potential (M-estimator) [24, 25, 26]. Then, the global optimum can be computed by alternating iterations of the w–weighted Gauss-Seidel update formula [24, 25]:

$$p(x) = \frac{S_k(x)C_k(x)w(x) + \lambda \sum\limits_{x' \in \mathcal{N}_x} \left[f_k(x') + p(x') - f_k(x) \right]}{S_k(x)^2 w(x) + \lambda\,\sharp\mathcal{N}_x + \gamma},$$
$$(22)$$

and a closed formula for updating w. That, in our case, we choose V as the Fiar potential [26], thus:

$$w(x) = \frac{\beta}{\beta + |C_k(x) - S_k(x)p(x)|}; \qquad (23)$$

where β is a positive parameter that establishes the outliers sensitivity.

In our experiments we use $\beta = 0.1$ and we denote with $\hat{f}_R$ the refined phase with our robust procedure.

3. Discussion on Related Work

3.1. Gabor Filters and the Short Time Fourier Transform

A Gabor filter can be understood as the convolution of the FP with a complex filter made up of the product of the

complex exponential $\exp(-i\,\omega x)$ with a low-pass Gaussian filter, G—where $i \stackrel{def}{=} \sqrt{-1}$. The complex response of a Gabor filter, tuned to the frequency ω, is computed as follows:

$$GF\{I\}(x;\omega) = I(x) \otimes [\exp(-i\,\omega x)G(x,\sigma)] \qquad (24)$$

where $\otimes$ denotes the convolution. It is common that the Gaussian width σ (consequently, the filter window size) depends on the frequency. That is, $\sigma \stackrel{def}{=} [\sigma_1(\omega_1), \sigma_2(\omega_2)]$ are filter scale–parameters in the image dimensions x_1 and x_2, respectively. A GFB is a set of Gabor filters defined by the set of respective frequencies $\{\omega^{(1)}, \omega^{(2)}, \dots, \omega^{(K)}\}$. Thus, for a given neighbourhood around the pixel x', the Gabor filter (24) with maximal response [magnitude of $GF\{I\}(x';\omega^*)$] is obtained when the filter frequency ω^* approximates the local FP frequency $\omega(x)$: $\omega^* \approx \omega(x')$ [13, 27].

(a) (b)

(c) (d)
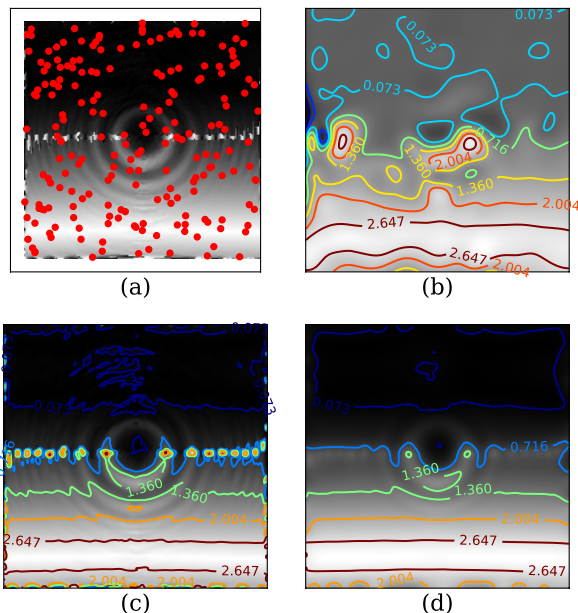
Figure 2: Illustration of filtering procedures for the initial differential phase f shown in panel 1f. a) Samples $\{x_j\}$ for the RBF based interpolation. Phases smoothed with b) the RBF-interpolation (f_{rbf}), c) the membrane filter (f_M) and with the proposed method ($\hat{f}$).

In general, the filter bank of this form is expressed by the Short Time Fourier Transform (STFT) [28, 29, 30]; which we write in the following form:

$$STFT\{I\}(x;\omega,\sigma,G) = [I(x)\exp(-i\,\omega x)] \otimes G(x,\sigma). \quad (25)$$

In STFT, the particular selection of the window G defines the filter.

We note that, if a Gaussian window is selected for the STFT, its response (for the proper frequency and bandwidth) only differs on the multiplicative phase term $\exp(i\,\omega x)$ from the GF. see Appendix A for the proof to this claim. In such case, the local frequency detector based on the maximal magnitude response of a GFB or the STFT

providing a proper parameter selection. Indeed, both approaches (Gabor filters or STFT) has been used for estimating local, absolute, frequency maps in interferometric FP with closed fringes [13, 14, 31].

3.2. Alternative Filtering Methods

The phase refining method proposed in subsection 2.2 can be seen as a filtering post-process to the initial differential phase computed with (11). However, this could be a simplistic interpretation of the importance of the refining procedure that builds upon the data term that keeps consistency between the resultant differential phases, $\{\hat{f}_k\}_{k=2,3,\dots,K}$, and the normalised FPs, $\{\cos(\psi_k)\}_{k=2,3,\dots,K}$. To clarify our claim, in the experiments we compare the performance of our proposal with two strategies that directly filter the initial differential phase maps, $\{f_k\}$. The alternatives do not take into account the normalised FPs. Thus, they are prone to introducing large deviation in the phase. Our comparison is not exhaustive: we intend to point our the importance of filtering the phase by preserving the consistency with the normalised FPs, rather than with initial differential phases alone; as a classical filtering process.

We evaluate a Radial Basis Function based interpolation and a membrane filter. By sampling the phase map and interpolating such samples with an RBF technique, we try to reduce the chance of selecting points with large structured error. Meanwhile, the membrane filter differs from our proposal in the data attachment term.

RBF Interpolation. A computationally efficient method for filtering noisy versions of smooth functions is to interpolate scattered samples with Radial Basis Functions (RBF) [32]. The procedure consists in sampling the phase map and and interpolating such samples with the RBF. Here, we denote by $\mathcal{S} = \{x_j\}_{j=1,2,\dots,N} \subset \mathcal{L}$ the sample (random subset) of pixels in the reticula space. Thus, the filtered local phase map, f_{rgb}, is computed as

$$f_{rgb}^{(k)}(x) = \sum_{j=1}^{N} h_j(x)\,\alpha_j^{(k)} + r_k(x), \quad \forall x \in \mathcal{L}, \qquad (26)$$

where r_k is a residual (it includes noise and the model limitations, model bias) and h is given by the multiquadric kernel [33]:

$$h_j(x) = \sqrt{d_j(x)/\kappa + 1}, \qquad (27)$$

where $d_j(x) = \|x - x_j\|^2$, x_j the centre of the jth basis function and κ a parameter that controls the smoothness of the interpolation. In our experiments, we set κ equal to the average of the square distance between sampled points $\{x_j\}$. Since the residual r_x is not Gaussian, we need the RBF to be made robust. Hence, the contribution $\alpha^{(k)}$ of the jth basis function is computed by minimising the ridge–regularised quadratic potential:

$$\alpha^{(k)} = \arg\min_{\alpha} \|A\,\alpha - y^{(k)}\|^2 + \lambda_R \|\alpha\|^2, \qquad (28)$$

5
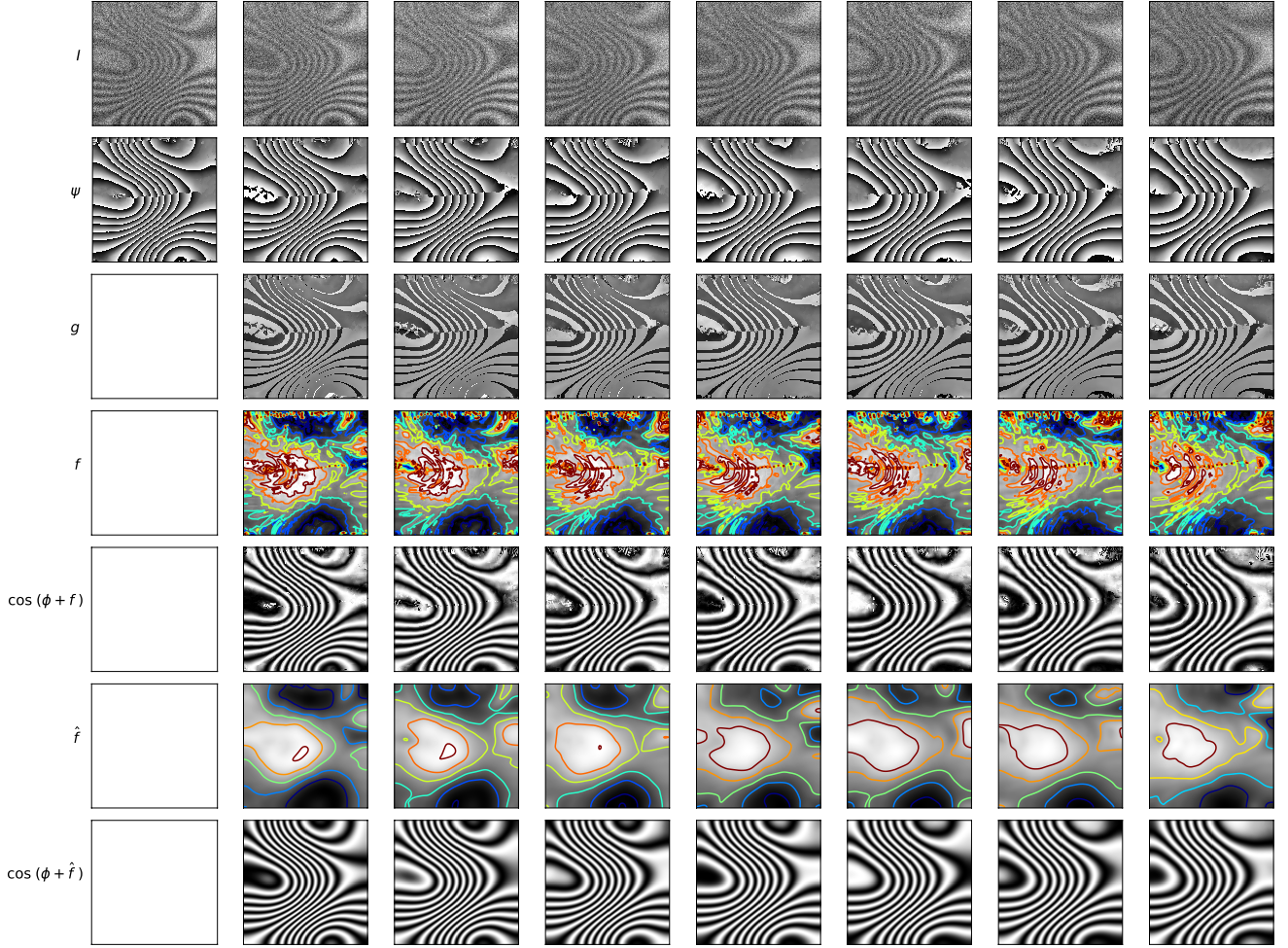
Figure 3: Top row, test FP sequence. Second row, local phase maps ψ_k computed with the GFB. Third row, phase difference $\psi_k - \psi_{k-1}$. Fourth row, initial differential phase $|\mathcal{W}\{\psi_k - \psi_{k-1}\}|$. Fifth row, reconstructed FP with the phase in the fourth row (displayed for comparison purpose). Sixth row, refined differential phase with the **proposed method** and, last row, corresponding reconstructed FP sequence (displayed for comparison purpose).

where λ_R is a positive parameter (ridge regression's parameter) that controls the smoothing process;

$$y_i^{(k)} \stackrel{def}{=} g_k(x_i). \tag{29}$$

and A is, in general, a symmetric and positive semidefinite matrix [34, 35]; with

$$[A]_{ij} \stackrel{def}{=} h_j(x_i). \tag{30}$$

Hence, we compute the coefficients with

$$\alpha^{(k)} = M \, y^{(k)} \tag{31}$$

where

$$M \stackrel{def}{=} [A\,A + \lambda_R I]^{-1} A. \tag{32}$$

Note that we can precompute M owing to its independence on k.

To illustrate the method, we show in panel (a) in Figure 2 depicts the pixels sampled; the initial phase corresponds

to the shown in Fig 1f. The filtered phase using RBF based interpolation is shown in Fig. 2b and the levelset shows a smooth reconstruction.

Membrane Filter. In order to compute the filtered version f_M of the noisy map f, one can use a membrane filter. In this case, the filtered map is computed by minimising the quadratic cost function:

$$f_M^{(k)} = \arg\min_m \sum_{x \in \mathcal{L}} \left\{ \left[m(x) - f_k(x)\right]^2 \right.$$
$$\left. + \lambda_M \sum_{x' \in \mathcal{N}_x} \left[m(x) - m(x')\right]^2 \right\}, \tag{33}$$

where the positive parameter λ_m controls the solution's smoothness. The minimisation of (33) can be achieved by iterating a Gauss-Seidel scheme with the updating formula:

$$m(x) = \frac{f_k(x) + \lambda_M \sum_{x' \in \mathcal{N}_x} m(x')}{1 + \lambda_M \sharp \mathcal{N}_x}. \tag{34}$$

The Panel (c) in Figure 2 shows the result of apply the
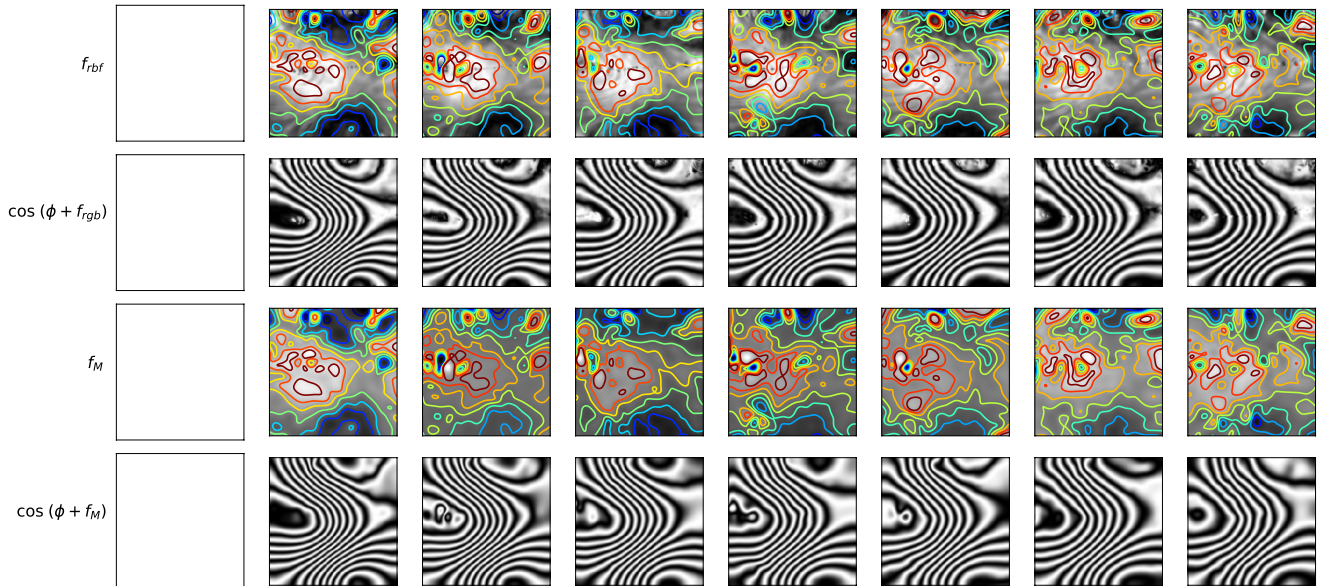
Figure 4: Top row, filtered phase differences using the **membrane** filter and (second row) reconstructed FP sequence. Third row, filtered phase differences using an **RBF** interpolation and (fourth row) reconstructed FP sequence.

membrane filter to the initial phase in Fig 1f. The levelset shows that large residuals associated with sign changes $(s_k - s_{k-s})$ are not completely clean out. For illustration purposes, Panel (d) depicts the refined phase computed with the proposed that seems to produce results of better quality: the quantitative evaluation of the methods' performance is presented in next Section.

4. Experiment

Figure 3 shows a simulated ESPI sequence. The first row depicts the interferograms generated with the model

$$I_k(x) = \big| b(x)\cos(\eta(x) + k\delta) - b(x)\cos(\eta(x) + \phi_k(x) + k\delta)\big|, \tag{35}$$

where η is randomly generated with a large variance uniform distribution. The second row shows the corresponding phase computed with the GFB (note the sign ambiguity). The third row shows the differences between consecutive phases $g_k = \psi_k - \psi_{k-1}$. The fourth row shows the initial differential phase f_k with (11). Since $f_k \in [0,\pi)$, it is unwrapped. We can note that despite the initial differential phase presents large errors at regions around the critical points (i.e. the point of zero frequency), they are filtered out by our phase refinement. For illustration purposes, the fifth row shows the reconstructed and filtered FPs computed as the cosine of the true synthetic phase in the acquisition at time $k - 1$ and the initial differential phase: $\cos(\phi_{k-1} + f_k)$. Compare the FP structure with the original in the first row. The residual noise in this reconstructed FP sequence is the effect of the residual r_k in our simplified model (9). The sixth row shows the refined phase differences and the last row shows the reconstructed FP sequence with $\cos(\phi_{k-1} + \hat{f}_k)$. The additional

parameters used in the experiments were the following: test images of 256×256 pixels, GFB tuned as in Ref. [13], RBF interpolation with $N = 200$ samples, regularisation parameters in (18) were set $\gamma = 1$ and $\lambda = 10$.

In order to demonstrate the suitablility of our refinement process, we compare our method with two phase filtering strategies: a membrane filter and an RBF based interpolation. Both strategies directly smooth out the initial differential phase without considering the FP structure. The data corresponds to the fourth row in the Figure 3 and the filtered results are shown in Figure 4. The first row shows the filtered phases with a membrane filter and the second row the reconstructed FP. The third row shows the filtered phases with the RBF interpolation and the fourth row shows the corresponding reconstructions.

Figures 3 and 4 depict the results of a single Monte Carlo experiment of 100 simulations with the same sequence and independent noise realisations. The errors for the reconstructed FP sequence are shown in the boxplots in Figure 5. We can observe that, consistently, the mean of the Mean Absolute Error (MAE) for the initial differential phase is reduced with the filtering methods, and the best results are obtained by our proposal. In our opinion, Figure 5 is very informative of our method capabilities. It depicts MAE, variances, extreme values and cases with error out of range. It also illustrated the method's behaviour across the time, an important feature when analysing transient phenomena.

In case the reader is interested in computing an estimate of the absolute phases ϕ, then a reference phase ϕ_a is required. Thus, the differential phases are integrated using

$$\tilde{\phi}_b(x) = \sum_{k=a}^{b} f_k(x) + \phi_a(x) \tag{36}$$
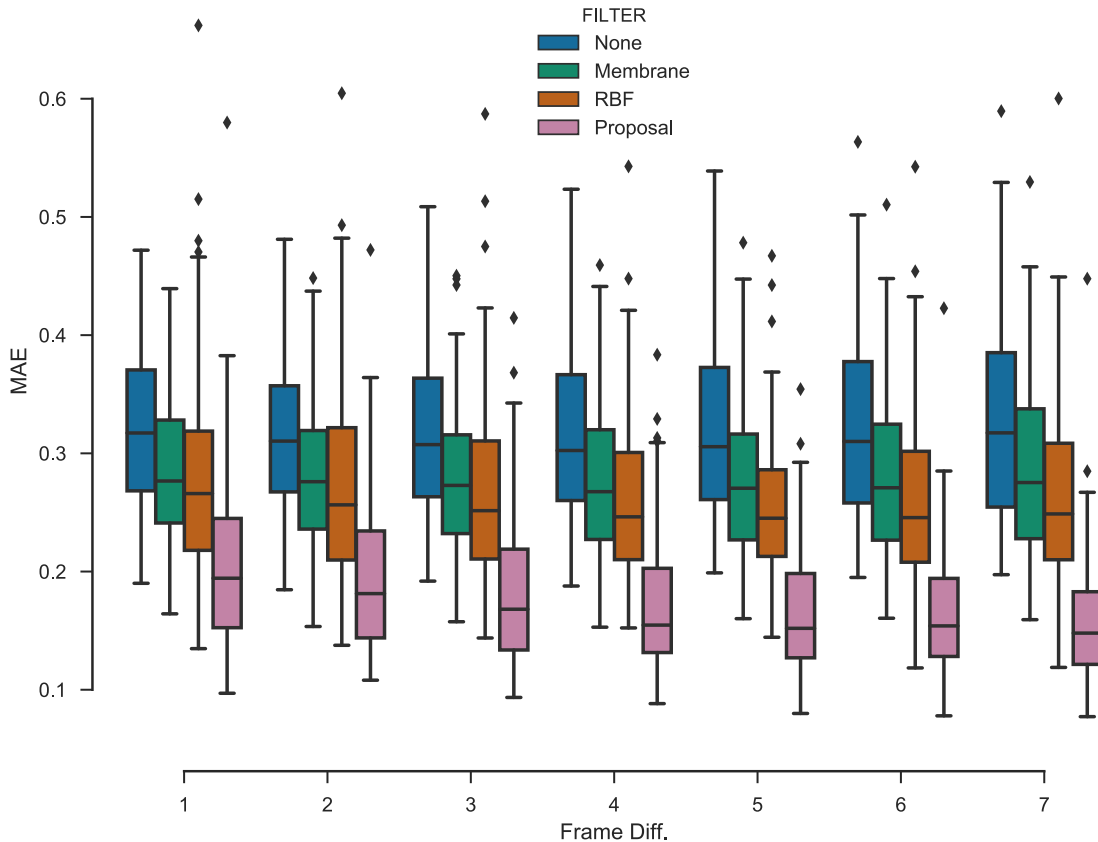
Figure 5: Summary of 100 Monte Carlo experiments for differential phase reconstructions of the FP sequence in Figure 3. The boxplots depict the distributions of the Mean Absolute Error (MAE) with respect the ground truth (synthetic data). **None** corresponds to the initial differential phase computed with (11). **Membrane** corresponds to filter the initial differential phase with the membrane filter. **RBF** corresponds to the results using the RBF based interpolation and **Proposal** corresponds to the refined solution computed with our method.

For example, the reference phase could be computed using a method in Refs. [15, 16, 17, 18, 19, 20, 21] in the case the FP presents closed fringes. The computation of the reference phase is beyond the scope the present work

Last experiment is conducted in a sequence acquired at 20,000 fps rate. It records, with an out–of–plane sensible ESPI experimental setup, the deformations of a hammered steel plate. The environmental conditions produced fringes of poor quality: low contrast, background inhomogeneity and highly noisy. First row in Figure (6) shows three FPs, second row shows the computed phases with the GFB. Note the effect of the random sign map, regions with incorrect phase by fringes' contrast loss and noise moles that could not be filtered out. Third row shows the initial differential phase, f. Despite the one can recognise a propagation pattern in form of wave expanding from the image centre, there are large phase moles corresponding to unfiltered noise. Such phase moles are not eliminated by the refining process as is shown in the results depicted in fourth row; the phase moles induce correlated artefacts in the refined phase, $\hat{f}$. In order to consider the moles as phase outliers, the data term in the refinement phase must be robust. The robust refined phase $\hat{f}_R$ computed with the procedure proposed in subsection 2.3 is shown in

row fifth.

5. Conclusions

We have presented a method for analysing FPs sequence. Our contribution is given by the computation of an initial differential phase based on a GFB and a refinement process. Two variants of the refinement stage are proposed: one based on a quadratic regularised (18) that is adequate for cases where the initial differential phase estimate is close to the true phase and a half-quadratic regularised (21) that fit for cases where the initial differential phase estimate is corrupted with outliers.

Our method allows us to analyse FP sequences of transient phenomena acquired with ESPI standard systems. It may provide an advantage in industrial applications where the experimental control is limited and sophisticated ESPI acquisition setups are hard to implement. The experimental evidence demonstrated that our method can be applied to noisy, time–varying illumination components and complex FPs with closed fringes. Such characteristics made the method suitable for the analysis of ESPI sequences of transient phenomena, providing FPs with contiguous
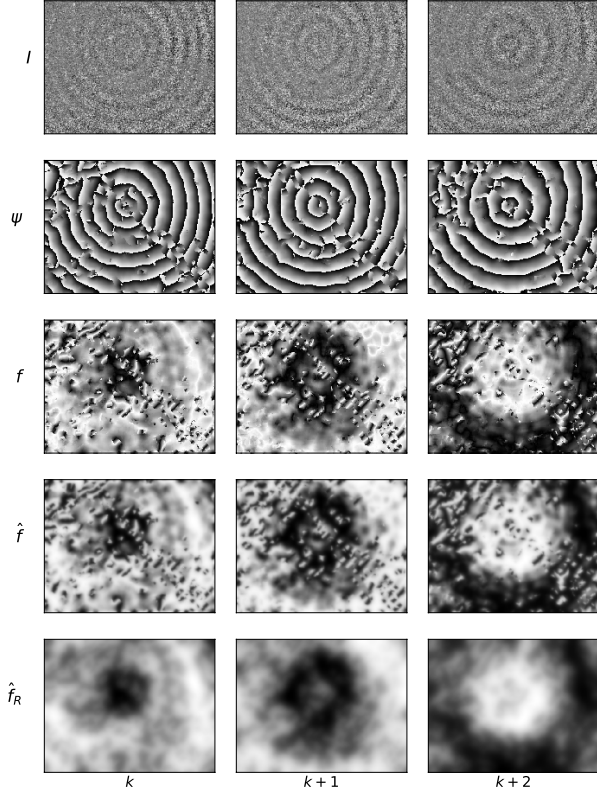
Figure 6: Differential phase recovered from real transient ESPI sequence, see text.

smooth phase difference and dynamic range in the interval $[0, \pi)$.

The experiments demonstrated that our phase refinement process [based on the minimisation of (18)] effectively enforces consistency of the solution with the FP and induces small corrections in order to maintain the validity of the first–order Taylor approximation. By contrast, if one filters the initial phase a large error may be introduced in the final phase; see experiments with the filter membrane (33) and the RBF interpolation. The experiments are computed with the Gauss-Seidel scheme (19) for the case of the quadratic energy and and for the half–quadratic energy alternating a Gauss-Seidel iteration with a weights w update [24, 25]. Future work will focus on developing efficient minimisation methods to improve overall performance. For example, we are interested in multigrid approaches such that reported in [36].

Acklowledgments

Appendix A

Since the operations are pixelwise, we omit the dependence on x in the corresponding variables the sake of notation simplicity.

Proof of Proposition 1. First we note that $\mathcal{W}\{\mathcal{W}\{x\} - \mathcal{W}\{y\}\} = \mathcal{W}\{x - y\}$. This relies on the definition of the wrap operator $\mathcal{W}\{x\} \stackrel{def}{=} x + 2\pi n$ for an integer n such that $\mathcal{W}\{x\} \in [-\pi, \pi)$. Indeed,

$$\mathcal{W}\{\mathcal{W}\{x\} - \mathcal{W}\{y\}\} = [[x + 2\pi n_1] - [y + 2\pi n_2]] + 2\pi n_3$$
$$= [x - y] + 2\pi \tilde{n} = \mathcal{W}\{x - y\}, \quad (37)$$

for some integers n_1, n_2 and n_3. Thus, the integer $\tilde{n} = n_1 - n_2 + n_3$ directly wraps $x - y$. Hence, by using (4), the wrapped phase difference gives

$$\mathcal{W}\{\psi_k - \psi_{k-1}\} = \mathcal{W}\{s_k[\phi_k + k\delta] + \tilde{\eta}_k$$
$$- s_{k-1}[\phi_{k-1} + (k-1)\delta] - \tilde{\eta}_{k-1}\}$$
$$= \mathcal{W}\{s_k\phi_k + s_k k\delta + \tilde{\eta}_k$$
$$- s_{k-1}\phi_{k-1} - s_{k-1}(k-1)\delta - \tilde{\eta}_{k-1}$$
$$- s_k\phi_{k-1} + s_k\phi_{k-1} - s_k\delta + s_k\delta\}$$
$$= \mathcal{W}\{s_k(\phi_k - \phi_{k-1}) + s_k\delta$$
$$+ (s_k - s_{k-1})[\phi_{k-1} + (k-1)\delta]$$
$$+ \tilde{\eta}_k - \tilde{\eta}_{k-1}\},$$
$$= \mathcal{W}\{s_k[\mathbf{f}_k + \delta] + \hat{\eta}_k\}, \quad (38)$$

where we use (2) and the define the residual

$$\hat{\eta}_k \stackrel{def}{=} (s_k - s_{k-1})[\phi_{k-1} + (k-1)\delta] + \tilde{\eta}_k - \tilde{\eta}_{k-1} \quad (39)$$

that absorbs the contribution of the residuals $(\tilde{\eta}_k, \tilde{\eta}_{k-1})$ and the change in the sign–map $(s_k - s_{k-1})$. Now apply the wrapping operator, we have

$$\mathcal{W}\{\psi_k - \psi_{k-1}\} = s_k[\mathbf{f}_k + \delta] + \hat{\eta}_k + 2\pi n_k, \quad (40)$$

where n_k is a field of integers. $\qquad \square$

Proof of Proposition 2. From (6), we have

$$0 \le f_k = |s_k[f_k + \delta] + \hat{\eta}_k + 2\pi n_k| \le \pi. \quad (41)$$

Recall that if $a \ge 0$, that $0 \le |a + b| \le a + |b|$. Thus,

$$f_k = f_k + \delta + r_k \le f_k + \delta + |\hat{\eta}_k + 2\pi n_k|. \quad (42)$$

for a residual r_k. The residual r_k in (42) is difficult to characterise with a particular probability density distribution. However, it fulfils

$$0 \le f_k + \delta + r_k \le \min\{\pi, f_k + \delta + |\hat{\eta}_k + 2\pi n_k|\}. \quad (43)$$

$\qquad \square$

Relationship of Gabor Filters and the STFT. We use the definition of the convolution, (24) and (25). Thus, we have

$$GF\{I\}(x;\omega) = \int_{-\infty}^{\infty} I(\tau) \exp[-i\,\omega(x-\tau)]G(x-\tau,\sigma)\,d\tau$$

$$= \exp[-i\,\omega x]\int_{-\infty}^{\infty} I(\tau)\exp[i\,\omega\tau]G(x-\tau,\sigma)\,d\tau$$

$$= \exp[-i\,\omega x]\,STFT\{I\}(x;\omega,\sigma,G) \tag{44}$$

Hence, a Gabor filter is the particular case of a coefficient of the STFT when the Gaussian window is selected and its response is multiplied by the phase factor: $\exp[-i\,\omega x]$. $\square$

References

[1] A. J. Moore, D. P. Hand, J. S. Barton, J. D. C. Jones, Transient deformation measurement with electronic speckle pattern interferometry and a high-speed camera, Appl. Opt. 38 (7) (1999) 1159–1162.

[2] P. K. Rastogi, Digital Speckle Pattern Interferometry & Related Techniques, John Wiley & Sons, Inc., New York, NY, USA, 2000.

[3] I. M. D. la Torre, M. del Socorro Hernández Montes, J. M. Flores-Moreno, F. M. Santoyo, Laser speckle based digital optical methods in structural mechanics: A review, Optics and Lasers in Engineering 87 (2016) 32 – 58.

[4] J. M. Huntley, G. H. Kaufmann, D. Kerr, Phase-shifted dynamic speckle pattern interferometry at 1 khz, Appl. Opt. 38 (31) (1999) 6556–6563.

[5] D. Hernandez, G. Atondo-Rubio, C. Lopez, J. Michel, Temporal evolution measurement of harmonic vibration induced over a rectangular plate using a high-speed ESPI system, Journal of Optoelectronics and Advanced Materials 17 (1-2) (2015) 216–221.

[6] X. Li, Z. Huang, M. Zhu, H. Zhang, X. Li, Measurement of transient deformation using high-speed temporal speckle pattern interferometry, Guangxue Xuebao/Acta Optica Sinica 35 (6).

[7] T. Hastie, T. Tibshirani, J. H. Friedman, The Elements of Statistical Learning: Data Mining, Inference, and Prediction, 2nd ed., ch 7, Springer, New York, NY USA, 2009.

[8] K. Ishikawa, K. Yatabe, N. Chitanont, Y. Ikeda, Y. Oikawa, T. Onuma, H. Niwa, M. Yoshii, High-speed imaging of sound using parallel phase-shifting interferometry, Opt. Express 24 (12) (2016) 12922–12932.

[9] K. Creath, Phase-shifting speckle interferometry, Appl. Opt. 24 (18) (1985) 3053–3058.

[10] A. Gonzalez, M. Servin, J. C. Estrada, J. A. Quiroga, Design of phase-shifting algorithms by fine-tuning spectral shaping, Opt. Express 19 (11) (2011) 10692–10697.

[11] K. Yatabe, K. Ishikawa, Y. Oikawa, Improving principal component analysis based phase extraction method for phase-shifting interferometry by integrating spatial information, Opt. Express 24 (20) (2016) 22881–22891.

[12] P. Etchepareborda, A. Bianchetti, A. L. Vadnjal, A. Federico, G. H. Kaufmann, Simplified phase-recovery method in temporal speckle pattern interferometry, Appl. Opt. 53 (30) (2014) 7120–7128.

[13] M. Rivera, O. Dalmau, A. Gonzalez, F. Hernandez-Lopez, Two-step fringe pattern analysis with a Gabor filter bank, Opt. Lasers Eng. 85 (2016) 29 – 37.

[14] Q. Kemao, Two-dimensional windowed Fourier transform for fringe pattern analysis: principles, applications and implementations, Optics and Lasers in Engineering 45 (2) (2007) 304–317.

[15] M. Servin, J. L. Marroquin, F. J. Cuevas, Fringe-follower regularized phase tracker for demodulation of closed-fringe interferograms, J. Opt. Soc. Am. A 18 (3) (2001) 689–695.

[16] M. Rivera, Robust phase demodulation of interferograms with open or closed fringes, J. Opt. Soc. Am. A 22 (6) (2005) 1170–1175.

[17] R. Legarda-Saenz, M. Rivera, Fast half-quadratic regularized phase tracking for nonnormalized fringe patterns, J. Opt. Soc. Am. A 23 (11) (2006) 2724–2731.

[18] J. C. Estrada, M. Servin, J. L. Marroquín, Local adaptable quadrature filters to demodulate single fringe patterns with closed fringes., Opt. Express 15 (5) (2007) 2288–2298.

[19] O. S. Dalmau-Cedeño, M. Rivera, R. Legarda-Saenz, Fast phase recovery from a single closed-fringe pattern, J. Opt. Soc. Am. A 25 (6) (2008) 1361–1370.

[20] L. Kai, Q. Kemao, Improved generalized regularized phase tracker for demodulation of a single fringe pattern, Opt. Express 21 (20) (2013) 24385–24397.

[21] M. Trusiak, Ł. Służewski, K. Patorski, Single shot fringe pattern phase demodulation using Hilbert-Huang transform aided by the principal component analysis, Opt. Express 24 (4) (2016) 4221–4238.

[22] O. Dalmau, M. Rivera, A. Gonzalez, Phase shift estimation in interferograms with unknown phase step, Opt. Commun. 372 (2016) 37 – 43.

[23] K. Yatabe, K. Ishikawa, Y. Oikawa, Simple, flexible, and accurate phase retrieval method for generalized phase-shifting interferometry, Journal of the Optical Society of America A: Optics and Image Science, and Vision 34 (1) (2017) 87–96.

[24] M. J. Black, A. Rangarajan On the unification of line processes, outlier rejection, and robust statistics with applications in early vision, Int. J. Comput. Vision, 19 (1) (1996) 57–91.

[25] M. Rivera, J. L. Marroquin, Half-quadratic cost functions for phase unwrapping, Opt. Lett. 29 (5) (2004) 504-506

[26] R. He, B. Hu, X. Yuan, L. Wang, Robust Recognition via Information Theoretic Learning. Springer, Amsterdam, The Netherlands, 2014.

[27] W. Jun, A. Asundi, Strain contouring with Gabor filters: filter bank design, Appl. Opt. 41 (34) (2002) 7229–7236.

[28] R. Schafer, L. Rabiner, Design and simulation of a speech analysis-synthesis system based on short-time Fourier analysis, IEEE Transactions on Audio and Electroacoustics 21 (3) (1973) 165–174.

[29] J. B. Allen, L. R. Rabiner, A unified approach to short-time Fourier analysis and synthesis, Proc. IEEE 65 (11) (1977) 1558–1564.

[30] J. Allen, Short term spectral analysis, synthesis, and modification by discrete Fourier transform, IEEE Transactions on Signal Processing 25 (3) (1977) 235–238.

[31] Q. Kemao, Windowed Fourier transform for fringe pattern analysis, Appl. Opt. 43 (13) (2004) 2695–2702.

[32] D. Broomhead, D. Lowe, Multivariable functional interpolation and adaptive networks, Complex Systems 2 (1988) 321–355.

[33] G. E. Fasshauer, J. G. Zhang, On choosing "optimal" shape parameters for RBF approximation, Numerical Algorithms 45 (1) (2007) 345–368.

[34] C. A. Micchelli, Interpolation of scattered data: Distance matrices and conditionally positive definite functions, Constructive Approximation 2 (1) (1986) 11–22.

[35] G. B. Wright, Radial basis function interpolation: Numerical and analytical developments, Ph.D. Thesis, University of Colorado at Boulder, Boulder, CO, USA, aAI3087597 (2003).

[36] M. Rivera, F. J. Hernandez-Lopez, A. Gonzalez, Phase unwrapping by accumulation of residual maps, Optics and Lasers in Engineering 64 (0) (2015) 51–58.

[37] J. D. Hunter, Matplotlib: A 2d graphics environment, Computing In Science & Engineering 9 (3) (2007) 90–95.